HHS Public Access

Author manuscript

J Pharm Sci. Author manuscript; available in PMC 2015 October 19.

Published in final edited form as:

J Pharm Sci. 2009 August ; 98(8): 2731–2746. doi:10.1002/jps.21630.

Budesonide nanoparticle agglomerates as dry powder aerosols with rapid dissolution

Nashwa El-Gendy[1], **Eric M. Gorman**[1], **Eric J. Munson**[1], and **Cory Berkland**[1,2,*]

[1]Department of Pharmaceutical Chemistry, The University of Kansas, Lawrence, KS 66047

[2]Department of Chemical and Petroleum Engineering, The University of Kansas, Lawrence, KS 66047

Abstract

Purpose—Nanoparticle technology represents an attractive approach for formulating poorly water soluble pulmonary medicines. Unfortunately, nanoparticle suspensions used in nebulizers or metered dose inhalers often suffer from physical instability in the form of uncontrolled agglomeration or Ostwald ripening. In addition, processing such suspensions into dry powders can yield broad particle size distributions. To address these encumbrances, a controlled nanoparticle flocculation process has been developed.

Method—Nanosuspensions of the poorly water soluble drug budesonide were prepared by dissolving the drug in organic solvent containing surfactants followed by rapid solvent extraction in water. Different surfactants were employed to control the size and surface charge of the precipitated nanoparticles. Nanosuspensions were flocculated using leucine and lyophilized.

Results—Selected budesonide nanoparticle suspensions exhibited an average particle size ranging from ~160–230 nm, high yield and high drug content. Flocculated nanosuspensions produced micron-sized agglomerates. Freeze-drying the nanoparticle agglomerates yielded dry powders with desirable aerodynamic properties for inhalation therapy. In addition, the dissolution rates of dried nanoparticle agglomerate formulations were significantly faster than that of stock budesonide.

Conclusion—The results of this study suggest that nanoparticle agglomerates possess the microstructure desired for lung deposition and the nanostructure to facilitate rapid dissolution of poorly water soluble drugs.

Keywords

nanoparticles; Budesonide; asthma; aerosol

1. Introduction

Pulmonary dosage forms have established an important role in the local treatment of lung diseases. Systemic treatments delivered through the lungs are also emerging since this route

To whom correspondence should be addressed. The University of Kansas, 2030 Becker Drive, Lawrence, KS 66047. Phone: (785) 864-1455. Fax: (785) 864- 1454. berkland@ku.edu.

offers access to a well blood-supplied surface area, avoids first-pass metabolism, and reduces drug degradation that may occur in the gastrointestinal tract (1, 2). Pulmonary drug delivery approaches continue to develop rapidly in an effort to improve product stability and efficacy for local and systemic treatment of diseases (3, 4). One problem with pulmonary drug delivery is the poor deposition efficiency as, in some cases, only approximately 10% of the inhaled drug powder reaches the alveoli (2). In addition, many current and emerging formulations would benefit from improved drug dissolution rate, which often enhances drug bioavailability.

In recent years, significant effort has been dedicated to expand nanotechnology for drug delivery since it offers a potential means of improving the delivery of small molecule drugs, as well as macromolecules such as proteins, peptides or genes to the tissue of interest (5). The increase in the percentage of poorly water-soluble molecules being identified as active pharmaceutical ingredients beckons new approaches to bring these molecules to the market place in a timely fashion (6). Nanoparticles, whether amorphous or crystalline, offer an interesting way of formulating drugs having poor water solubility (7). By presenting drugs at the nanoscale, dissolution can be rapid and as a result the bioavailability of poorly soluble drugs can be significantly improved (8, 9). Nanoparticles have been disregarded to some extent in dry powder dosage forms because particles < 1 μm have a high probability of being exhaled before deposition, are prone to particle growth due to Ostwald ripening and can suffer from uncontrolled agglomeration (4, 10–12). Conversely, particles exhibiting an aerodynamic diameter from 1 to 5 μm are more likely to bypass the mouth and throat, resulting in augmented deposition in the lung periphery (11, 13).

Budesonide is a potent nonhalogenated corticosteroid with high glucocorticoid receptor affinity, airway selectivity and prolonged tissue retention. It inhibits inflammatory symptoms, such as edema and vascular hyperpermeability (14). Budesonide is already applied through dry powder inhalers (DPI, Pulmicort), metered dose inhalers (pMDI, Rhinocort) or ileal-release capsules (Entocort) (15). This drug is considered one of the most valuable therapeutic agents for the prophylactic treatment of asthma despite its poor solubility in water (21.5 μg/ml under constant agitation) (16).

The objective of this study was to translate budesonide nanosuspensions into dry powder formulations capable of effective deposition and rapid dissolution. Different surfactants were used to create surface charge on the nanoparticles and charge interactions were leveraged to flocculate nanoparticles into nanoparticle agglomerates exhibiting a particle size range of ~2–4 μm. Nanoparticle suspensions were evaluated by measuring particle size, polydispersity and zeta potential. Nanosuspensions were then flocculated and lyophilized to obtain dry powders composed of micron-sized agglomerates. Nanoparticle agglomerates were characterized by the determination of particle size, aerolization efficiencies, flowability characteristics, process yield and loading efficiency. Finally, dissolution studies were performed for the selected nanoparticles and nanoparticle agglomerates, which were compared with the stock drug. The present work represents an approach to harmonize the features of micro- and nanostructure for developing novel dry powder aerosols.

2. Materials and methods

2.1. Materials

Budesonide (Bud), L-α-phosphatidylcholine (lecithin; Lec), cetyl alcohol (CA), L-leucine (Leu), polyvinylpyrrolidone (PVP), sorbitan tri-oleate (Span 85) and sodium chloride were purchased from Sigma Chemicals Co, USA. Pluronic F-127 (PL, Mw ~12,220) was purchased from BASF, The Chemical Company, USA. Polyvinyl alcohol (PVA; Mw = 22,000, 88% hydrolyzed) was purchased from Acros Organics, New Jersey, USA. Potassium dihydrogen phosphate, disodium hydrogen phosphate, acetone, ethanol and acetonitrile were purchased through Fisher Scientic. Floatable dialysis membrane units (Mw cut-off = 10,000 Da) were obtained from Spectrum Laboratories Inc., USA. A549 cells were obtained from the American Type Culture Collection (ATCC, Rockville, MD). The cell culture medium (Ham's F-12 Nutrient Mixture, Kaighn's modified with L-glutamine) was purchased through Fisher Scientic. Fetal bovine serum (FBS) was purchased from Hyclone. Penicillin-streptomycin was purchased from MB Biomedical, LLC. Trypsin- EDTA was purchased through Gibco. MTS reagent [tetrazolium compound; 3-(4,5-dimethylthiazol-2-yl)-5-(3-carboxymethoxyphenyl)-2-(4-sulfophenyl)-2H-tetrazolium, inner salt] was purchased from Promega, USA. Double-distilled water was used throughout the study, provided by an EASYpure® RODI (Barnstead International, Model # D13321).

2.2. Preparation of budesonide nanosuspensions

Nanosuspensions were prepared using a precipitation technique. Briefly, solutions of budesonide in acetone were prepared at concentrations of 0.1 and 0.2% w/v and water was used as nonsolvent. To precipitate the drug, the solution of budesonide was directly injected into the non-solvent at a rate of 1 mL/min under sonication (Fisher Scientic, Sonic Dismembrator) with an amplitude of 46% in an ice bath. The selected surfactants for the study included hydrophobic (cetyl alcohol and Span 85), hydrophilic (PL, PVA and PVP) and amphoteric (lecithin). The hydrophobic and amphoteric surfactants were added to the drug organic solvent solution and the contents were allowed to stand at room temperature for 30 to 45 minutes with occasional vortexing to allow complete solubilization of the drug and the surfactants. Hydrophilic surfactants were added to the aqueous phase. Surfactants were used individually or in combination as reported.

2.3. Flocculation of budesonide nanoparticles

The budesonide nanoparticle agglomerates were prepared by slow addition of L-leucine solution (1 % w/v) in water to flocculate nanoparticle suspensions during homogenization at 25,000 rpm for 30 sec. The amount of L-leucine added was adjusted to a drug:leucine ratio equal to 1:1. The size of budesonide nanoparticle agglomerates was measured in Isoton diluent using a Coulter Multisizer 3 (Beckman Coulter Inc.) equipped with a 100 μm aperture after three hours of incubation with the flocculating agent. The flocculated suspensions were kept overnight at room temperature to allow evaporation of acetone and then frozen at −80° C and transferred to a freeze dryer (Labconco, FreeZone 1). Drying lasted for 36 hours to remove all appreciable water content. Lyophilized powder was stored at room temperature for further characterization

2.4. Characterization of the prepared nanoparticles and nanoparticle agglomerates

2.4.1. Particle size analysis and Zeta potential measurement of the selected nanosuspensions—The size and zeta potential of the nanosuspensions were determined by dynamic light scattering (Brookhaven, ZetaPALS). Zeta potential measurements were performed using 1 mM KCl solution. All measurements were performed in triplicate.

2.4.2. Determination of particle size distribution and aerodynamic diameter of the prepared nanoparticle agglomerates—The particle size of the dispersed nanoparticle agglomerates as well as the resuspended lyophilized powder was measured using a Coulter Multisizer 3. The aerodynamic size distributions of the agglomerate powders were measured directly from lyophilized powder by time-of-flight measurement using an Aerosizer LD (Amherst Instruments) equipped with a 700 μm aperture operating at 6 psi.

2.4.3. Aerosolization of nanoparticle agglomerates—Aerodynamic characteristics of selected nanoparticle agglomerates were studied in vitro using a Tisch Ambient Cascade Impactor (Tisch Environmental, Inc., Ohio). The study was carried out by applying ~20 mg powder manually into the orifice of the instrument at three air flow rates; ~15 L/min, ~30 L/min and ~60 L/min. Cut-off particle aerodynamic diameters at 30 L/min for each stage of the impactor were: pre-separator (10.00 μm), stage 0 (9.00 μm), stage 1 (5.8 μm), stage 2 (4.7 μm), stage 3 (3.3 μm), stage 4 (2.1 μm), stage 5 (1.1 μm), stage 6 (0.7 μm), stage 7 (0.4 μm) and filter (0 μm). Nanoparticle agglomerates deposited on each stage of the impactor were determined by measuring the difference in weight of filters placed on the stages. The mass median aerodynamic diameter, MMAD, and geometric standard deviation, GSD, were obtained by a linear fit of the cumulative percent less-than the particle size range by weight plotted on a probability scale as a function of the logarithm of the effective cut-off diameter (17, 18).

2.4.4. Transmission electron microscopy (TEM)—Image data was used to corroborate the size of nanoparticles and nanoparticle agglomerates and to observe their morphological aspects. Transmission electron micrographs (TEM) were obtained for budesonide nanoparticles and nanoparticle agglomerates using a JEOL 1200 EXII transmission electron microscope. Initially, carbon-coated grids (Electron Microscopy Sciences) were floated on a droplet of the suspensions on a flexible plastic film (Parafilm), to permit the adsorption of the particles onto the grid. After this, the grid was blotted with a filter paper and air dried for 1 hr.

2.4.5. SSNMR analysis—All ^{13}C spectra were collected using a Chemagnetics CMX-300 spectrometer using ramped amplitude cross-polarization (RAMP) (19), magic-angle spinning (MAS) (20), and SPINAL-64 decoupling (21). Samples were packed in 7 mm zirconia rotors using Teflon® end caps, and spun at 4 kHz in a 7 mm spin module from Revolution NMR.

All spectra are the sum of 2,000–48,000 transients collected using a 1–1.5 s pulse delay, a contact time of 0.5–2 ms, and a ^{1}H 90° pulse width of 3–4.5 μs. The free induction decays consisted of 512–2048 points with a dwell time of 33.3 μs. The spectra were externally

referenced to tetramethylsilane using the methyl peak of 3-methylglutaric acid at 18.84 ppm (22).

The assignment of the peaks in the ^{13}C spectrum of the "as received" budesonide was performed using the modified spectral editing methods of Hu et al. (23) and the ^{13}C solution predictions from ChemBioDraw Ultra (version 11.0) from CambridgeSoft and ACD/CNMR Predictor (version 7.09) from ACD/Labs. The spectral editing subspectra were collected using the parameters given in Table I. These parameters were optimized using 3-methylglutaric acid.

2.4.6. Determination of process yield—The lyophilized powder for the prepared nanoparticle agglomerates was weighed and the yield was calculated using the following expression:

$$\%\,\text{Process yield} = \frac{\text{Recovered mass}}{\text{Mass entered into the experiment}} \times 100$$

2.4.7. Budesonide loading efficiency measurement—Budesonide loading efficiency was assessed by dispersing one mg of the lyophilized powder in 10 mL ethanol. The dispersion was sonicated in a bath-type sonicator (Branson 3510) for 2 hours and then kept overnight at room temperature to allow complete dissolution of the drug by ethanol. Then the solution was centrifuged (Beckman, Avanti ™) at ~15,000 rpm for 30 min to remove insoluble surfactants and L-leucine and the amount of drug in the supernatant was determined spectrophotometrically (Agilent C) at 243 nm. Drug loading was defined as follows:

$$\%\,\text{Loading} = \frac{\text{Recovered budesonide mass}}{\text{Total mass}} \times 100$$

2.4.8. Flowability characteristics—The flow properties of the nanoparticle agglomerates were assessed by angle of repose (tan θ = height/radius) measurement of the dried powders (24). The fixed- height cone method was used. A glass funnel with cut stem surface of 5 mm internal diameter was fixed at 2.5 cm height over a flat surface. The powders were allowed to flow gently through the funnel until a cone was formed and reached the funnel orifice. The flow of powder was then stopped and the average diameter of the formed cone (D) was measured. The area of the base of the cone was taken as a measure of the internal friction between the particles. The angle of repose was calculated by the equation: tan θ = height/radius.

In addition, the bulk density, Hausner ratio (Tapped density/bulk density) and Carr's index (C_i) [(Tapped density − bulk density)/ Tapped density X 100%] were also determined for the dried powders (24, 25). Five mg of powders were weighed and poured into a 10 mL graduated measuring cylinder. The bulk volume occupied (V_b) was recorded. The measuring cylinder was tapped until a constant value was obtained and the tapped volume was recorded (V_t). The process was repeated at least three times and the average was taken in each case.

The bulk and tapped densities of powder were calculated by dividing the weight by the corresponding bulk volume or tapped volume recorded.

2.5. Dissolution studies

The dissolution of the prepared nanoparticles and nanoparticle agglomerates was determined and compared with the dissolution characteristics of the stock drug. The dissolution of budesonide was carried out at 37 ± 0.5°C in a 400 mL beaker. A known amount (~10 mg) of the lyophilized powder was suspended in 10 mL phosphate buffered saline (PBS, pH 7.4) and was placed into a floatable dialysis membrane unit (Mw cut-off = 10,000 Da), and the unit was allowed to float in a beaker containing 300 mL of PBS. The solution was stirred at a constant speed (100 rpm) using a magnetic stirrer (Barnstead, Thermolyne MIRAK™). At predetermined time intervals for a total period of 8 hours, aliquots (5 ml) of the medium were removed and fresh medium was immediately added to continue the dissolution study. Studies were conducted in triplicate. The budesonide concentration was analyzed using a reverse-phase HPLC method. A Shimadzu HPLC system including a solvent delivery pump (Shimadzu LC-10AT), a controller (Shimadzu SCL-10A), an autoinjector (Shimadzu SIL-10AxL), and a UV detector (Shimadzu SPD-10A) was used in this study. The peak areas were integrated using Shimadzo Class VP (Version 4.3). A 4.6 mm × 100 mm long Zorbax SB C-18 column (Agilent C) with a particle diameter of 3.5 μm was used. During the assay, budesonide was eluted isocratically at a mobile phase flow rate of 0.6 mL/minute and monitored with a UV detector operating at 254 nm. The mobile phase for the assay consisted of an acetonitrile and water mixture (45:55 v/v) (2). The run time for the assay was 20 minutes, and the retention time for budesonide was 14.01 minutes.

2.6. Cytotoxicity assay

The cytotoxicity of selected nanoparticles and nanoparticle agglomerates was assessed using the CellTiter 96® Aqueous Cell Proliferation Assay (Promega) and compared with stock budesonide, lecithin, leucine, physical mixtures of these ingredients and blank nanoparticle agglomerates. In this experiment, 8×10^4 A549 cells/well were seeded in 96-well microtiter plates. At the end of the incubation period (12 h), 20 μl of MTS reagent solution was added to each well and incubated for 3 h at 37 °C. The absorbance was measured at 490 nm using a microtiter plate reader (SpectraMax, M25, Molecular Devices Corp., CA). The percentage of viable cells with all tested concentrations was calculated relative to untreated cells (26, 27).

3. Results and discussion

3.1. Fabrication of budesonide nanoparticles

Various methods have been reported for generating nanoparticles of poorly water soluble drugs (8, 28, 29). A precipitation method was selected to produce budesonide nanoparticles. Different concentrations of the drug and various types and ratios of surfactants, individually or in combination, were evaluated as a means to control the particle size and surface charge. Surfactants were chosen from excipients regarded as suitable for inhalation that have been designated as safe for human use (3). Formulations prepared using PVP and PVA in different ratios produced very large particle sizes even when combined with other

surfactants. The mean particle size of formulations containing lecithin, cetyl alcohol, Span 85 and/or PL ranged from ~130 to 323 nm. Formulations containing Span 85 alone or in combination with lecithin yielded the smallest particle size but since Span is liquid at room temperature, it was not suitable for use in dry powder formulations.

Attempts to generate budesonide nanoparticles using PL alone or in combination with lecithin yielded reasonable particle sizes (~129–270 nm) but offered very low nanoparticle yields and high polydispersity values (30). Selected surfactant combinations for preparing budesonide nanosuspensions in acetone were designated F1 (0.1% w/v Bud + 0.02% w/v Lec), F2 (0.1% w/v Bud + 0.02% w/v CA + 0.01% w/v PL) and F3 (0.2% w/v Bud + 0.04% w/v CA + 0.02% w/v PL) as reported in Table II. These surfactant combinations demonstrated small particle size and could be used in dry powder formulations. A small change in zeta potential was observed with different types of surfactants and the values ranged from 22.5–25.1 mV (Table III). The charged surface of the nanoparticles provided the potential for destabilizing this colloid via interaction with a flocculating agent to form nanoparticle agglomerates.

3.2. Agglomerated budesonide nanoparticles yielded desirable aerosol characteristics

The mechanism to control nanoparticle agglomeration is mainly driven by leveraging the competitive processes of attraction (van der Waals force) and repulsion (electrostatic repulsive force or steric hindrance barrier or both). If particles are mainly stabilized electrostatically, disruption of the electrostatic double layer surrounding the particles will result in the agglomeration of nanoparticles (31). The addition of flocculating agents has also been speculated to decreases the cohesion between particles. It is thought that these agents may interfere with weak bonding forces between small particles, such as Van der Waals and Coulomb forces. These agents may act as weak links or “chain breakers” between the particles which are susceptible to disruption in the turbulent airstream created during inhalation (3, 32). The amino acid, L-leucine, used as a flocculating agent in these studies may also act as an anti-adherent material to yield a high respirable fraction of the agglomerated budesonide nanoparticles (33).

Flocculation of nanoparticles resulted in the formation of agglomerates within the micrometer or sub-micrometer scale consisting of closely-packed nanoparticles (34). Nanoparticle agglomerates were prepared through the slow incorporation of a flocculating agent (L-leucine) during homogenization (25,000 rpm) for 30 sec. The geometric size distribution of the prepared nanoparticle agglomerates was measured in Isoton diluent using a Coulter Multisizer 3. The size average of the three selected nanoparticle agglomerate formulations ranged from ~2–4 μm (Table IV). The size distributions of resuspended lyophilized powders were slightly broader and the average particle size was slightly increased, when compared to the nanoparticle agglomerates prior to lyophilization (Table IV and Fig. 1). This may be due to the deposition of nanoparticles on agglomerates during lyophilization or to cohesion between agglomerates as a result of drying. The key physical parameter that predicts the site of aerosol deposition within the lungs for particles larger than several hundred nanometers is the aerodynamic diameter (d_{aero}) (35). The aerodynamic diameter of the flocculated nanoparticles, measured by an Aerosizer LD, was smaller than

the geometric diameter and the aerodynamic size distribution was narrower than the geometric size distribution (Table IV and Fig. 2). When compared to the geometric diameter, the lower aerodynamic diameter was likely due to the low density of nanoparticle agglomerates.

The theoretical mass–mean aerodynamic diameters (d_{aero}) of the nanoparticle agglomerates, determined from the geometric particle size and tapped density, was found to be 2, 2.1 and 2.5 μm for F1, F2 and F3, respectively as calculated from the relationship (36):

$$d_{aero} = \frac{d_{geo}}{\gamma}\sqrt{\rho/\rho_a}$$

Where d_{geo} = geometric diameter, γ = shape factor (for a spherical particle, $\gamma = 1$; for aerodynamic diameter calculations, the particles in this study were assumed to be spherical), ρ = particle bulk density and ρ_a = water mass density (1 g/cm^3). Tapped density measurements underestimate particle bulk densities since the volume of particles measured includes the interstitial space between the particles. The true particle density, and therefore the aerodynamic diameter of a given powder, is expected to be slightly larger than reported (37). Particles with a d_{aero} between 1 and 5 μm that are inhaled via the mouth are capable of efficient alveolar deposition, whereas d_{aero} between 4 and 10 μm are more likely to deposit primarily in the tracheobronchial region of the lungs (35). Therefore, the budesonide nanoparticle agglomerates with d_{aero} in the 2–2.5 μm range are expected to deposit primarily in the alveolar region of the lungs.

Aerosizer results and theoretical MMAD calculations were corroborated by cascade impaction studies at air flow rates of ~15 L/min, ~30 L/min and ~60 L/min (Fig. 3). At these flow rates, most nanoparticle agglomerates were deposited in stages 6 and 7 of the cascade impactor which was suggestive of efficient aerosolization and a high fine particle fraction. The aerosolization efficiency of nanoparticle agglomerates was represented by the percent emitted fraction (%EF), percent respirable fraction (RF), mass-median aerodynamic diameter (MMAD) and geometrical standard deviation (GSD). The percent emitted fraction was determined from the following equation:

$$\%\ \text{Emitted fraction}\ (\%EF) = \frac{\text{Total particle mass collected from the stages of the impactor}}{\text{Total particle mass entered into the impactor}} \times 100$$

The high emitted fraction of nanoparticle agglomerates obtained at the tested flow rates suggested efficient aerosolization of the powder (Table V). The percent respirable fraction (RF), referred to also as the fine particle fraction of the total dose (FPF_{TD}), was calculated as the percentage of aerosolized particles that reached the lower seven stages of the impactor (corresponding to aerodynamic diameters below 5.8 μm), or the lower five stages (corresponding to aerodynamic diameters below 3.3 μm) according to the following equation (17, 37):

$$\%\ \text{Respirable fraction (RF)} = \frac{\text{Powder mass recovered from terminal stages of the impactor}}{\text{Total particle mass recovered in the impactor}} \times 100$$

The results of the respirable fraction also suggested the efficient aerosolization of nanoparticle agglomerate powders (Table V) (38). The geometric standard deviation (GSD) of the nanoparticle agglomerates was determined from the following equation (35):

$$\text{GSD} = \left(\frac{d_{84.13\%}}{d_{15.87\%}}\right)^{1/2}$$

Where d_n is the diameter at the nth percentile of the cumulative distribution. The mass–mean geometric size of nanoparticle agglomerates ranged between 3 and 4 μm with a GSD of ~2.3 μm (Table V). Typical GSD values for aerosol particles are between 1.3–3.0 (17). The mass-mean aerodynamic diameter (MMAD) of the selected nanoparticle agglomerates, as calculated from the cascade impaction results (Table V) was close to that obtained from the Aerosizer (Table IV) although it was slightly smaller than the theoretical density values calculated from the tapped density indicating the suitability of the prepared nanoparticle agglomerate powders for peripheral lung deposition (i.e., < 3 μm).

Electron microscopy was used to study the morphology of budesobide nanoparticle and nanoparticle agglomerate formulations. Transmission electron micrographs (TEM) of F1 nanoparticles (Fig. 4A) depicted slightly elongated nanoparticles with smooth surfaces and a particle size around 170 nm. TEM images of F1 nanoparticle agglomerates (Fig. 4B) show that the nanoparticles were flocculated into micron sized agglomerates with irregular structure and some sharp edges.

Fig. 5. shows the ^{13}C spectra of budesonide by itself and in formulations. Both the budesonide as received and the leucine exhibit relatively narrow lines (several tens of hertz), indicating that these samples are crystalline. Lecithin also had narrow lines, which is consistent with it being a crystalline form of phosphatidylcholine; however, it is a semi-solid and therefore cannot be crystalline. Conversely the budesonide that was melt quenched had significantly broader lines (several hundreds of hertz) indicating that the budesonide is consistent with it being amorphous. In the nanoparticles, the peaks for budesonide are similar to the peaks in the budesonide that was melt quenched, although the peak at ~180 ppm shows that there is a small amount of crystalline budesonide in the nanoparticles. The tall, sharp peaks in the spectrum of the nanoparticle agglomerates align with the peaks in the leucine spectrum and showed that the leucine in the formulation has undergone phase separation and has crystallized to some extent. The peak at 180 ppm showed that the amount of crystalline budesonide had increased in the formulation of the nanoparticle agglomerates. This was consistent with the shape of several other budesonide peaks in the spectrum.

Budesonide consists of 25 carbons (Fig. 6); however, the spectrum of the budesonide as received had at least 27 resolved peaks and several peaks that may be the result of several

overlapping peaks. The extra peaks did not seem to be due to splitting, as would be expected if there were more than one molecule in the asymmetric unit cell.

The budesonide is a racemic mixture of both epimers that have been shown to pack differently in the crystal lattice (39). Therefore, spectral editing was used in an attempt to assign the peaks in the spectrum to determine if the differences in the two epimers could be used to explain the “extra” peaks. The spectral editing experiment allowed the assignment of carbon type (C, CH, CH_2, or CH_3) to a peak, these assignments could then be combined with predictions to assign the peaks to specific carbons within the molecule. The carbon type of most of the peaks could be assigned from these experiments (Fig. 7) with the exception of a few of the aliphatic peaks (particularly ~30–40 ppm). These results were then compared with predictions of the solution state chemical shifts from two different software programs and the resulting assignments are shown in Table VI. Chemical shifts for a compound in the solution and solid state can vary by as much as 10 ppm. For this reason, some assignments can be narrowed down to a few possibilities but an exact assignment was not possible with this data. For example, carbons 2 and 4 can be assigned to the peaks at 122.5 and 128.2, but it was not possible to definitively determine which carbon was associated with which peak. The solution predictions placed carbon 22 at ~103 ppm, while the spectral editing experiment showed that there are two peaks at 104.5 and 107.3 ppm that can be assigned to CH carbons. Additionally, carbon 22 is the chiral center of the epimers. Based on these observations and the fact that the two epimers have been shown to pack in different conformations, both peaks were assigned to carbon 22 with the interpretation that each peak represents one of the epimers. It is important to note that this interpretation assumes the budesonide is pure, which we have not confirmed. Additionally, there is always the possibility that these are different polymorphs; however, reports of polymorphism in budesonide have not been identified.

The process of agglomerating nanoparticles was evaluated to determine their yield. The results (Table IV) have shown that the process was efficient providing a high yield (~90–95%) and minimum batch variability. The loading efficiency of the drug in the prepared nanoparticle agglomerates was found to be between 85–95% (Table IV), thus demonstrating minimal loss of drug during formation.

The flow characteristics of the selected nanoparticle agglomerates were also determined (Table VII). Angle of repose, Hausner ratio and Carr’s index are considered to be indirect methods for quantifying powder flowability (24). Budesonide nanoparticle agglomerates generally exhibited similar bulk densities and lower tapped densities than that of the stock drug powder. Nanoparticle agglomerates also demonstrated improved flow properties. This may be attributed to the reduced denisity of the nanoparticle agglomerates. In addition, L-leucine has been reported to reduce surface energy in dry powders and may improve flowability in this case (40). Formula F3 showed slightly better flowability compared to the others according to the Carr’s index; however, all nanoparticle agglomerate powders possessed acceptable flowability.

3.3. Budesonide nanoparticle and nanoparticle agglomerates showed improved dissolution rates

A dissolution study of budesonide was conducted for the prepared nanoparticles and nanoparticle agglomerates and compared to the unprocessed drug. The cumulative percentage of drug dissolved after 8 hours (Q_{8h}) was found to be slower than that of the nanoparticles and faster than that of the stock budesonide (Table IV). This finding was the expected result of increasing the surface area by decreasing the particle size. F2 and F3 nanoparticle and nanoparticle agglomerate formulations showed faster drug dissolution than F1 which may be due to the incorporation of the hydrophilic surfactant, PL (Fig. 8). In addition, increasing the concentration of this surfactant (F3) led to even faster dissolution. Linear regression analysis of the dissolution data concluded that the drug was released by the Higuchi diffusion mechanism in all cases. A two-way Analysis of Variance (ANOVA) was performed to determine the significance of differences in dissolution kinetics. Significant differences ($\alpha = 0.05$) existed between nanoparticles, nanoparticle agglomerates and stock budesonide. No significant differences existed between different nanoparticles or nanoparticle agglomerate formulations. A significant improvement ($P<0.05$) in the dissolution behavior of the nanoparticles and nanoparticle agglomerates was also observed when these were individually compared to the stock budesonide.

3.4. Formulation components exhibited minimal cytotoxicity

The cytotoxicity of the different budesonide formulations were compared to stock budesonide, lecithin, leucine, physical mixtures of F1 components and blank F1 nanoparticle agglomerates (Fig. 9). Stock budesonide, excipients and physical mixtures of F1 components up to 5 mg/mL did not show any significant cytotoxicity in A549 cells at the end of 12 hours. Blank F1 nanoparticle agglomerates did induce a very low level of cytotoxicity where the IC_{50} was found to be 0.97 mg/mL. Additionally, F1 nanoparticles and nanoparticle agglomerates also induced very low level of cytotoxicity with IC_{50} values equal to 1.67 mg/mL and 1.91 mg/mL, respectively. The IC_{50} values occurred at higher concentrations than the maximum daily dose of inhaled budesonide currently prescribed. These results may suggest that lecithin was responsible for the cytotoxic effect.

4. Conclusion

Many current techniques to generate dry powder aerosols have a major disadvantage of poor control over the particle shape, size and size distribution. In addition, many pulmonary formulations may benefit from the improved bioavailability and rapid onset of action that may be achieved by using drug nanoparticles. In this work, budesonide nanosuspensions were successfully prepared yielding nanoparticles in the range of ~160–230 nm. This was accomplished by using surfactants proven to be safe for human use such as lecithin. Nanosuspensions were flocculated using L-leucine and the resulting nanoparticle agglomerates were analyzed. Nanoparticle agglomerates were efficiently aerosolized and offered a high fine particle fraction suitable for accessing the peripheral lung. Nanoparticle agglomerates also exhibited significantly faster budesonide dissolution when compared to the stock powder. In conclusion, budesonide nanoparticle agglomerates demonstrated a

desirable microstructure for efficient lung deposition and nanostructure for rapid dissolution of poorly water soluble drugs.

Acknowledgments

We would like to acknowledge support for this work from the Cystic Fibrosis Foundation, the Coulter Foundation, and the Higuchi Biosciences Center as well as additional lab funding from the American Heart Association, the NIH (R03 AR054035, P20 RR016443 and T32 GM08359-11) and the Department of Defense. In addition, we acknowledge the support of the NSF (CHE 0719464). We also thank Prof. C. Russ Middaugh for the use of laboratory equipment and The Microscopy Lab for assistance with electron microscopy.

References

1. Foster KA, Yazdanian M, Audus KL. Microparticulate uptake mechanisms of in-vitro cell culture models of the respiratory epithelium. J Pharm Pharmacol. 2001; 53:57–66. [PubMed: 11206193]
2. Rasenack N, Steckel H, Muller BW. Micronization of anti-inflammatory drugs for pulmonary delivery by a controlled crystallization process. J Pharm Sci. 2003; 92:35–44. [PubMed: 12486680]
3. Chougule MB, Padhi BK, Jinturkar KA, Misra A. Development of Dry Powder Inhalers. Recent Patents on Drug Delivery & Formulation. 2007; 1:11–21. [PubMed: 19075871]
4. Young PM, Chan HK, Chiou H, Edge S, Tee TH, Traini D. The influence of mechanical processing of dry powder inhaler carriers on drug aerosolization performance. J Pharm Sci. 2007; 96:1331–1341. [PubMed: 17455362]
5. Panyamand J, Labhasetwar V. Biodegradable nanoparticles for drug and gene delivery to cells and tissue. Adv Drug Deliv Rev. 2003; 55:329–347. [PubMed: 12628320]
6. Merisko-Liversidge E, Liversidge GG, Cooper ER. Nanosizing: a formulation approach for poorly-water-soluble compounds. Eur J Pharm Sci. 2003; 18:113–120. [PubMed: 12594003]
7. Lindfors L, Skantze P, Skantze U, Westergren J, Olsson U. Amorphous drug nanosuspensions. 3. Particle dissolution and crystal growth. Langmuir. 2007; 23:9866–9874. [PubMed: 17696457]
8. Rabinow BE. Nanosuspensions in drug delivery. Nat Rev Drug Discov. 2004; 3:785–796. [PubMed: 15340388]
9. Kesisoglou F, Panmai S, Wu Y. Nanosizing--oral formulation development and biopharmaceutical evaluation. Adv Drug Deliv Rev. 2007; 59:631–644. [PubMed: 17601629]
10. Lindfors L, Forssen S, Skantze P, Skantze U, Zackrisson A, Olsson U. Amorphous drug nanosuspensions. 2. Experimental determination of bulk monomer concentrations. Langmuir. 2006; 22:911–916. [PubMed: 16430248]
11. Shi L, Plumley CJ, Berkland C. Biodegradable nanoparticle flocculates for dry powder aerosol formulation. Langmuir. 2007; 23:10897–10901. [PubMed: 17894513]
12. Sepassi S, Goodwin DJ, Drake AF, Holland S, Leonard G, Martini L, Lawrence MJ. Effect of polymer molecular weight on the production of drug nanoparticles. J Pharm Sci. 2007; 96:2655–2666. [PubMed: 17696165]
13. Telkoand MJ, Hickey AJ. Dry powder inhaler formulation. Respir Care. 2005; 50:1209–1227. [PubMed: 16122404]
14. Kompella UB, Bandi N, Ayalasomayajula SP. Subconjunctival nano- and microparticles sustain retinal delivery of budesonide, a corticosteroid capable of inhibiting VEGF expression. Invest Ophthalmol Vis Sci. 2003; 44:1192–1201. [PubMed: 12601049]
15. Bandi N, Wei W, Roberts CB, Kotra LP, Kompella UB. Preparation of budesonide- and indomethacin-hydroxypropyl-beta-cyclodextrin (HPBCD) complexes using a single-step, organic-solvent-free supercritical fluid process. Eur J Pharm Sci. 2004; 23:159–168. [PubMed: 15451004]
16. Jacobs C, Muller RH. Production and characterization of a budesonide nanosuspension for pulmonary administration. Pharm Res. 2002; 19:189–194. [PubMed: 11883646]
17. Vanbever R, Ben-Jebria A, Mintzes JD, Langer R, Edwards DA. Sustained release of insulin from insoluble inhaled particles. Drug Development Research. 1999; 48:178–185.
18. Phamand S, Wiedmann TS. Note: dissolution of aerosol particles of budesonide in Survanta, a model lung surfactant. J Pharm Sci. 2001; 90:98–104. [PubMed: 11064383]

19. Metz G, Wu X, Smith SO. Ramped-amplitude cross polarization in magic-angle-spinning NMR. Journal of Magnetic Resonance, Series A. 1994; 110(2):219–227.
20. Stejskal EO, Schaefer J, Waugh JS. Magic-angle spinning and polarization transfer in proton-enhanced NMR. Journal of Magnetic Resonance (1969). 1977; 28:105–112.
21. Fung BM, Khitrin AK, Ermolaev K. An Improved Broadband Decoupling Sequence for Liquid Crystals and Solids. Journal of Magnetic Resonance. 2000; 142:97–101. [PubMed: 10617439]
22. Barich DH, Gorman EM, Zell MT, Munson EJ. 3-Methylglutaric acid as a ^{13}C solid-state NMR standard. Solid State Nuclear Magnetic Resonance. 2006; 30:125–129. [PubMed: 16887343]
23. Hu JZ, Harper JK, Taylor C, Pugmire RJ, Grant DM. Modified Spectral Editing Methods for ^{13}C CP/MAS Experiments in Solids. Journal of Magnetic Resonance. 2000; 142:326–330. [PubMed: 10648150]
24. Staniforth, JN. Powder flow. In: Aulton, ME., editor. Pharmaceutics: The Science of Dosage Form Design. Churchill Livingstone; London: 2002. p. 205-208.
25. Kumar V, Kothari SH, Banker GS. Compression, compaction, and disintegration properties of low crystallinity celluloses produced using different agitation rates during their regeneration from phosphoric acid solutions. AAPS PharmSciTech. 2001; 2:E7. [PubMed: 14727882]
26. Bandi N, Kompella UB. Budesonide reduces vascular endothelial growth factor secretion and expression in airway (Calu-1) and alveolar (A549) epithelial cells. Eur J Pharmacol. 2001; 425:109–116. [PubMed: 11502275]
27. Soundara Manickam D, Bisht HS, Wan L, Mao G, Oupicky D. Influence of TAT-peptide polymerization on properties and transfection activity of TAT/DNA polyplexes. J Control Release. 2005; 102:293–306. [PubMed: 15653153]
28. Govender T, Stolnik S, Garnett MC, Illum L, Davis SS. PLGA nanoparticles prepared by nanoprecipitation: drug loading and release studies of a water soluble drug. J Control Release. 1999; 57:171–185. [PubMed: 9971898]
29. Bilati U, Allemann E, Doelker E. Development of a nanoprecipitation method intended for the entrapment of hydrophilic drugs into nanoparticles. Eur J Pharm Sci. 2005; 24:67–75. [PubMed: 15626579]
30. Dailey LA, Schmehl T, Gessler T, Wittmar M, Grimminger F, Seeger W, Kissel T. Nebulization of biodegradable nanoparticles: impact of nebulizer technology and nanoparticle characteristics on aerosol features. J Control Release. 2003; 86:131–144. [PubMed: 12490379]
31. Kumar PV, Jain NK. Suppression of agglomeration of ciprofloxacin-loaded human serum albumin nanoparticles. AAPS PharmSciTech. 2007; 8:17. [PubMed: 17408217]
32. Murthy VS, Cha JN, Stucky GD, Wong MS. Charge-driven flocculation of poly(L-lysine)-gold nanoparticle assemblies leading to hollow microspheres. J Am Chem Soc. 2004; 126:5292–5299. [PubMed: 15099114]
33. Young PM, Cocconi D, Colombo P, Bettini R, Price R, Steele DF, Tobyn MJ. Characterization of a surface modified dry powder inhalation carrier prepared by “particle smoothing”. J Pharm Pharmacol. 2002; 54:1339–1344. [PubMed: 12396294]
34. Shi LJ, Berkland C. pH-Triggered dispersion of nanoparticle clusters. Advanced Materials. 2006; 18:2315–2315.
35. Fiegel J, Fu J, Hanes J. Poly(ether-anhydride) dry powder aerosols for sustained drug delivery in the lungs. J Control Release. 2004; 96:411–423. [PubMed: 15120898]
36. Vanbever R, Mintzes JD, Wang J, Nice J, Chen D, Batycky R, Langer R, Edwards DA. Formulation and physical characterization of large porous particles for inhalation. Pharm Res. 1999; 16:1735–1742. [PubMed: 10571280]
37. Fiegel J, Garcia-Contreras L, Thomas M, Verberkmoes J, Elbert K, Hickey A, Edwards D. Preparation and in vivo evaluation of a dry powder for inhalation of capreomycin. Pharm Res. 2008; 25:805–811. [PubMed: 17657592]
38. Chew NY, Shekunov BY, Tong HH, Chow AH, Savage C, Wu J, Chan HK. Effect of amino acids on the dispersion of disodium cromoglycate powders. J Pharm Sci. 2005; 94:2289–2300. [PubMed: 16136546]
39. Albertsson J, Oskarsson A, Svensson C. X-ray study of budesonide: Molecular structures and solid solutions of the (22S) and (22R) epimers of 11β,21-dihydroxy-16α,17α-

propylmethylenedioxy-1,4-pregnadiene-3,20-dione. Acta Crystallographica Section B. 1978; 34:3027–3036.

40. Shur J, Nevell TG, Ewen RJ, Price R, Smith A, Barbu E, Conway JH, Carroll MP, Shute JK, Smith JR. Cospray-dried unfractionated heparin with L-leucine as a dry powder inhaler mucolytic for cystic fibrosis therapy. J Pharm Sci. 2008:1–12. [PubMed: 17990322]

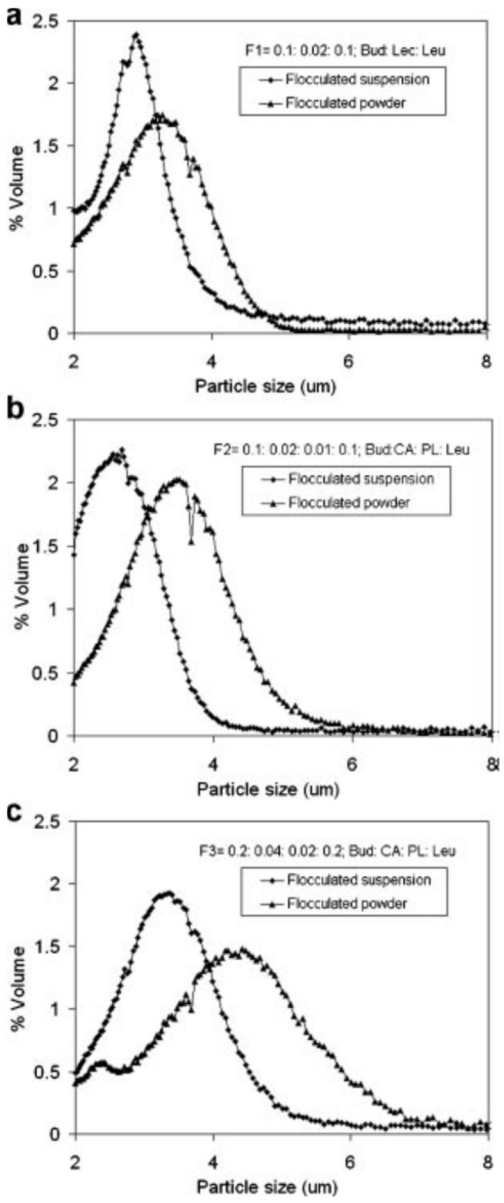

Fig. 1.

The particle size distributions of budesonide nanoparticle agglomerates in suspension after flocculation and resuspended after lyophilization.

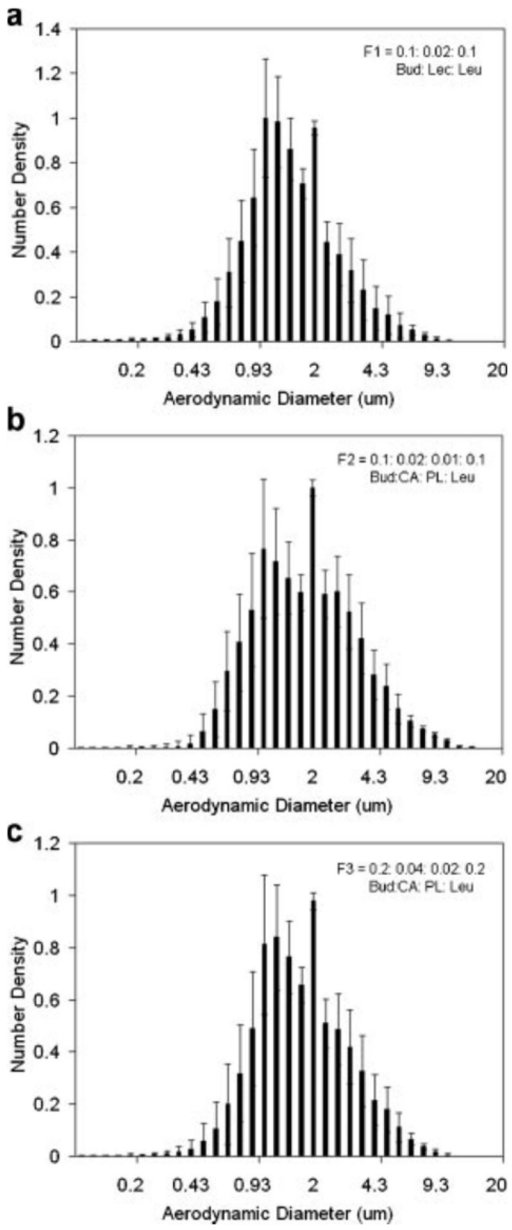

Fig. 2.

Aerodynamic size distributions of budesonide nanoparticle agglomerates after lyophilization.

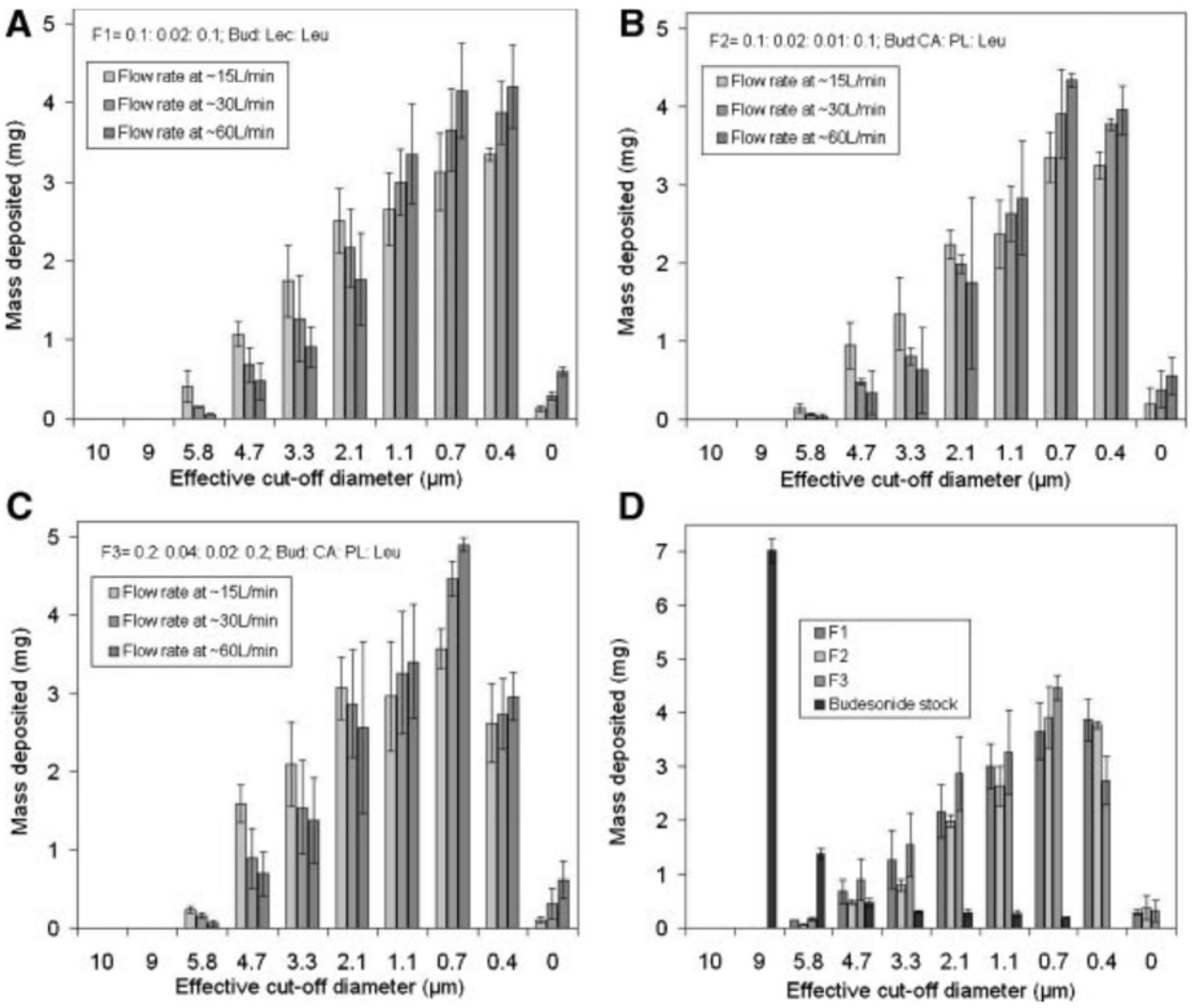

Fig. 3.

The distribution of budesonide nanoparticle agglomerate formulations (A) F1, (B) F2, and (C) F3 deposited on the stages of a cascade impactor. (D) Formulations were compared with stock budesonide at a flow rate of ~30 L/min.

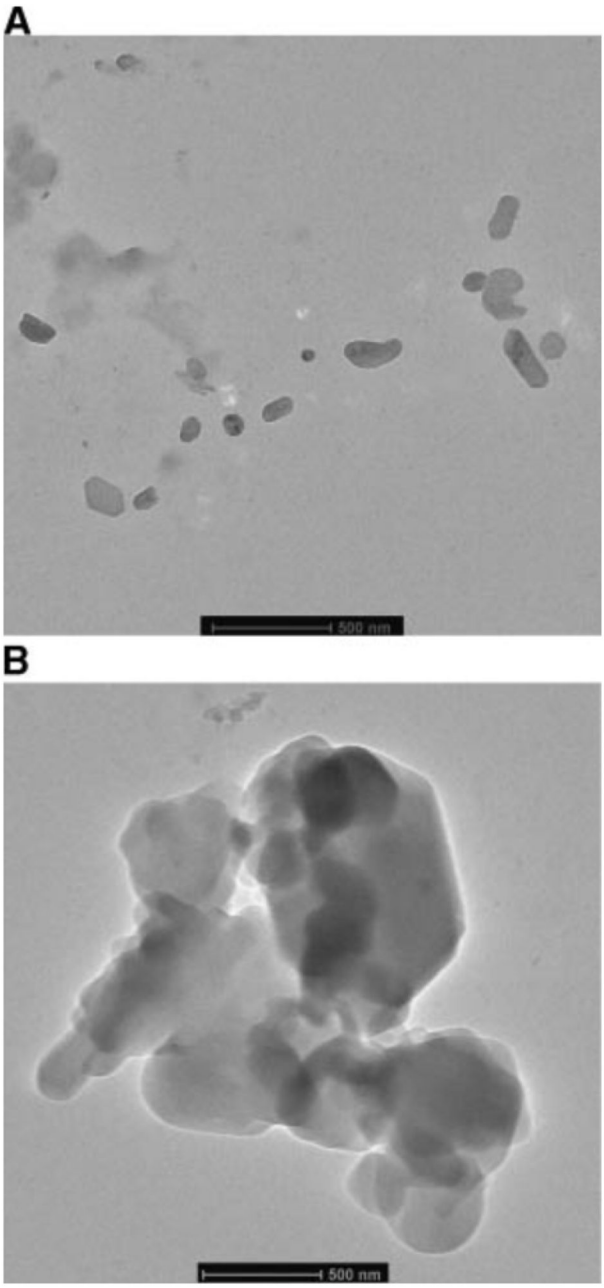

Fig. 4.
Transmission electron micrographs of A) F1 nanoparticles and B) F1 nanoparticle agglomerates.

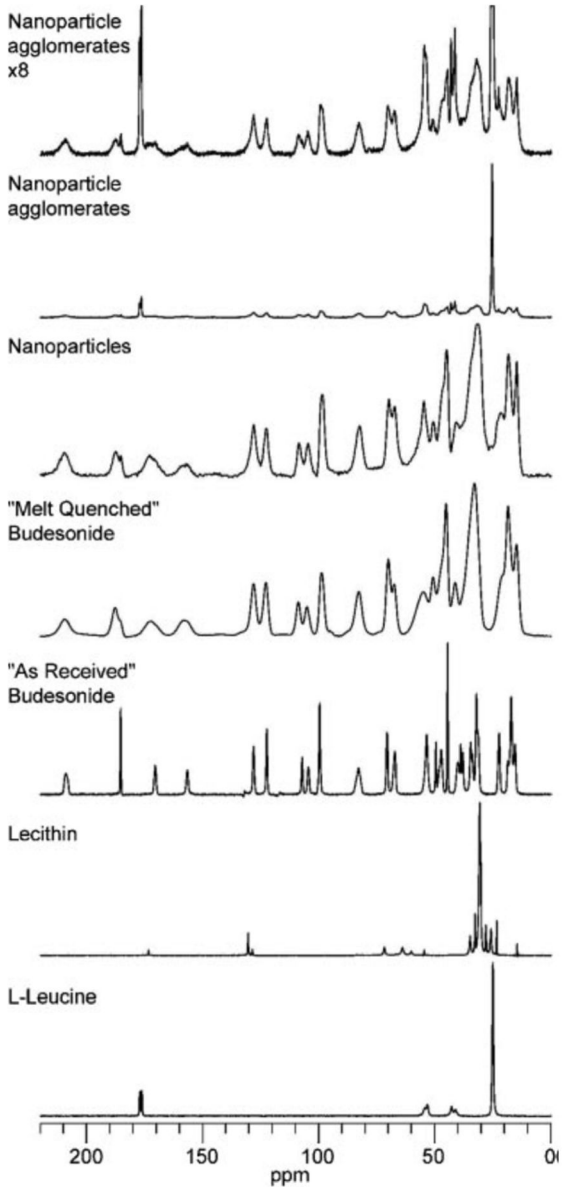

Fig. 5.

^{13}C CP/MAS spectra of budesonide, excipients, and budesonide formulations. The nanoflocs spectrum was expanded 8 times vertically to produce the nanoflocs x8 spectrum to aid the interpretation of the budesonide peaks.

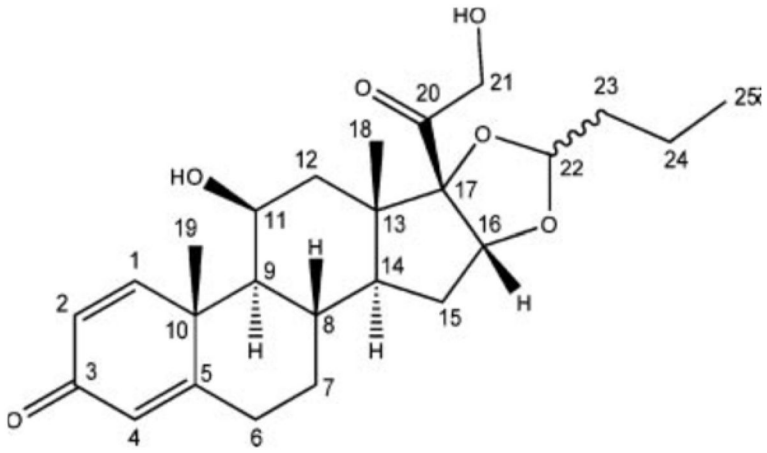

Fig. 6.
Structure of budesonide with carbon numbering.

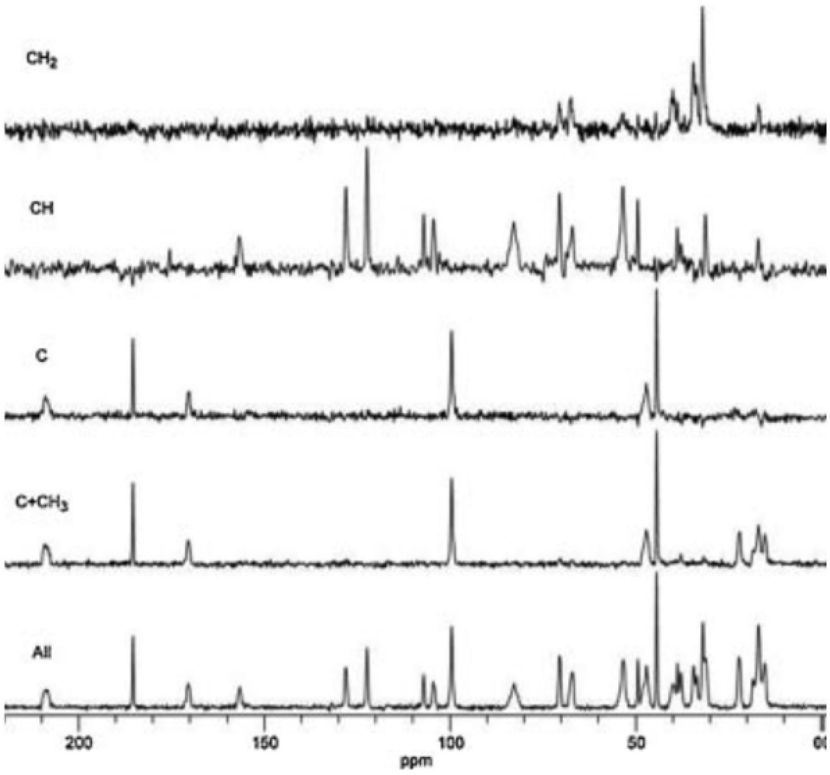

Fig. 7.

^{13}C CP/MAS spectra from spectral editing experiment.

All = all carbon types are shown, $C+CH_3$ = only unprotonated and methyl carbons are shown, C = only unprotonated carbons are shown, CH = only methine carbons are shown, and CH_2 = only methylene carbons are shown.

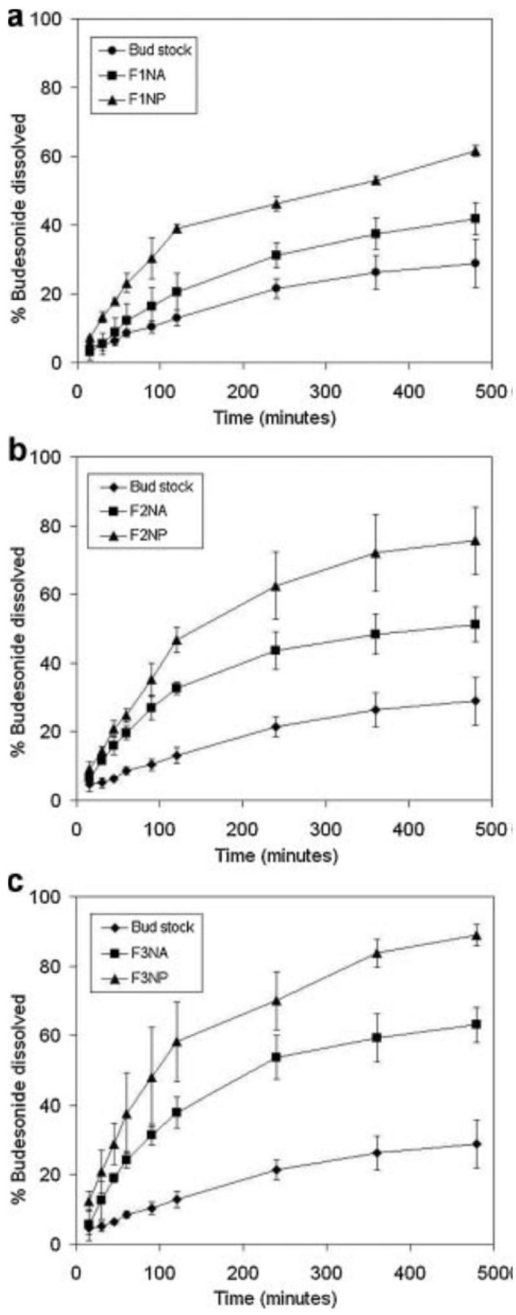

Fig. 8.

In-vitro dissolution profiles of budesonide in PBS (pH 7.4) from budesonide stock, nanoparticle formulations (NP) and nanoparticle agglomerate formulations (NA).

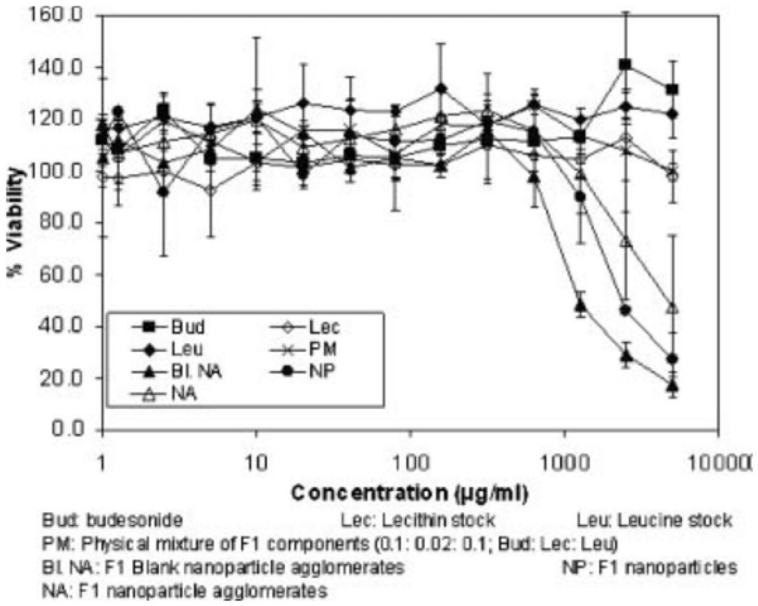

Fig. 9.

Viability of A549 cells in the presence of formulation components as determined by an MTS assay.

Table I

Parameters used to collect ^{13}C spectral editing subspectra.*

Subspectra	Pulse Sequence	t_{CP} (μs)	t_{PI} (μs)	t_{DD} (μs)	t_{SL} (μs)	Number of Transients
All	(+)	1500	0.2	—	133	800
C+CH_3	(+)	1500	0.2	130	3	800
C	(−)	400	135	130	3	8,000
CH	(+)	40	24	—	133	6,000
	(−)	37	0.2	130	1	6,000
CH2	(+)	80	39	—	133	6,000
	(−)	78	0.2	147	1	6,000

*All subspectra were collected with a 1.5 s pulse delay, a ^{1}H 90° pulse width of 3.1 μs, 1024 acquisition points with a dwell time of 33.3 μs, and a magic-angle spinning rate of 4 kHz.

Table II

Composition of the selected formulations.

Formulation	Budesonide (% w/v)	Lecithin (% w/v)	Cetyl alcohol (% w/v)	Pluronic F127 (% w/v)
F1	0.1	0.02		
F2	0.1		0.02	0.01
F3	0.2		0.04	0.02

Table III

Physical properties of budesonide nanoparticle (values = average ± S.D.).

Formulation	Nanoparticle size (nm)	Zeta-potential (mV)	Polydispersity
F1[a]	160.9 ± 15.6	25.1 ± 1.3	0.41 ± 0.1
F2[b]	188.8 ± 26.3	24.2 ± 1.1	0.34 ± 0.02
F3[c]	232.2 ± 11.2	22.5 ± 0.5	0.33 ± 0.02

[a] F1 = 0.1: 0.02; Bud: Lec

[b] F2 = 0.1: 0.02: 0.01; Bud: CA: PL

[c] F3 = 0.2: 0.04: 0.02; Bud: CA: PL

Table IV

Characteristics of budesonide nanoparticle agglomerates (values = average ± S.D.).

Characteristics	Formulations		
	F1[a]	F2[b]	F3[c]
Geometric particle size (μm) of NA[d] before lyophilization	2.8 ± 0.4	2.7 ± 0.4	3.2 ± 0.7
Geometric particle size (μm) of lyophilized NA[d]	3.1 ± 0.6	3.3 ± 0.7	3.9 ± 1.1
MMAD[f] of lyophilized NA[d]	1.4 ± 1.7	2.1 ± 1.8	1.9 ± 1.8
% Process yield of lyophilized NA[d]	95.5 ± 4.9	92.7 ± 3.1	89.7 ± 3.6
Loading Efficiency of lyophilized NA[d]	95.9 ± 3.6	86.5 ± 6.0	92.5 ± 6.6
Q_{8h}[g] NP[e]	61.5 % ± 1.6	75.5 % ± 9.9	88.9 % ± 3.0
Q_{8h}[g] NA[d]	41.8 % ± 4.6	51.2 % ± 5.1	63.1 % ± 5.1

[a] F1 = 0.1: 0.02; Bud: Lec

[b] F2 = 0.1: 0.02: 0.01; Bud: CA: PL

[c] F3 = 0.2: 0.04: 0.02; Bud: CA: PL

[d] NA: Nanoparticle agglomerates.

[e] NP: Nanoparticles.

[f] MMAD: Mass median aerodynamic diameter obtained from Aerosizer.

[g] Q_{8h}: % budesonide dissolved after 8 hours.

Table V

Cascade impaction results of lyophilized budesonide nanoparticle agglomerates (values = average ± S.D.).

Characteristics of the lyophilized NA[d]			**Formulations**		
			F1[a]	**F2[b]**	**F3[c]**
At flow rate of ~15 L//min	% EF[e]		74.9 ± 6.1	69.3 ± 5.5	86.5 ± 8.6
	% RF[f]	< 5.7	96.3 ± 1.8	97.5 ± 1.3	97.9 ± 0.3
		< 3.3	77.6 ± 3.9	81.2 ± 5.2	75.3 ± 1.7
	MMAD[g]		1.7 ± 0.1	1.5 ± 0.1	1.9 ± 0.3
	GSD[h]		2.4 ± 0.2	2.3 ± 0.1	2.3 ± 0.3
At flow rate of ~30 L//min	% EF[e]		75.3 ± 7.3	70.2 ± 4.1	81.2 ± 12.9
	% RF[f]	< 5.7	97.1 ± 0.2	96.8 ± 1.5	96.9 ± 1.4
		< 3.3	84.3 ± 3.9	87.7 ± 1.5	82.3 ± 4.2
	MMAD[g]		1.3 ± 0.2	1.2 ± 0.04	1.6 ± 0.3
	GSD[h]		2.3 ± 0.3	2.3 ± 0.4	2.3 ± 0.1
At flow rate of ~60 L//min	% EF[e]		77.4 ± 6.6	72.2 ± 5.9	82.9 ± 12.7
	% RF[f]	< 5.7	95.8 ± 0.2	95.9 ± 1.5	95.7 ± 1.7
		< 3.3	87.1 ± 2.3	89.3 ± 2.5	83.6 ± 2.8
	MMAD[g]		1.1± 0.2	1.1 ± 0.1	1.3 ± 0.2
	GSD[h]		2.3 ± 0.1	2.3 ± 0.2	2.3 ± 0.1

[a] F1 = 0.1: 0.02; Bud: Lec

[b] F2 = 0.1: 0.02: 0.01; Bud: CA: PL

[c] F3 = 0.2: 0.04: 0.02; Bud: CA: PL

[d] NA: Nanoparticle agglomerates.

[e] % EF: Percent emitted fraction.

[f] RF: Percent respirable fraction.

[g] MMAD: Mass median aerodynamic diameter.

[h] GSD: Geometric standard deviation.

Table VI

^{13}C peak assignments for budesonide as received.

Assignment	As Received	ACD/Labs*	ChemBioDraw*
20	209.0	207.0	211.2
3	185.4	186.2	185.7
5	170.6	170.3	168.1
1	156.7	156.5	158.4
2	122.5 and 128.2	127.5	128.3
4		122.1	124.2
22	104.5 and 107.3**	105.1	102.0
17	99.8	94.4	105.0
16	83.0	77.3	86.7
11	67.4 and 70.7	68.0	69.0
21		67.0	66.6
9	49.7 and 53.6	54.1	59.0
14		48.8	44.0
13	44.6 and 47.4	47.0	44.7
10		42.6	44.1
12	32.2, 33.9, 34.7, 38.1, 39.0, and 40.2	41.0	40.4
23		35.3	36.5
7		33.4	32.0
6		31.9	32.9
15		31.9	32.7
8	31.6	32.3	34.6
19	15.6, 18.7, and 22.5	21.0	19.0
18		16.3	17.3
25		14.0	14.4
24	17.2	18.4	13.1

* Software predictions of chemical shifts in solution.

** See text for explanation.

Table VII

Flowability characteristics of budesonide nanoparticle agglomerates (values = average ± S.D.).

Formula No.	Angle of repose (θ) (flowability)	Bulk density (g/cm^3)	Tapped density (g/cm^3)	Carr's index (C_i %)	Hausner ratio
F1 [a]	37.1 ± 2.6	0.34 ± 0.1	0.42 ± 0.03	21.8 ± 0.5	1.2 ± 0.03
F2 [b]	39.1 ± 1.1	0.31 ± 0.1	0.40 ± 0.1	23.6 ± 0.6	1.3 ± 0.03
F3 [c]	37.8 ± 2.1	0.29 ± 0.1	0.38 ± 0.1	18.6 ± 0.4	1.2 ± 0.1
Stock budesonide	43.5 ± 0.7	0.30 ± 0.04	0.47 ± 0.1	35.4 ± 2.1	1.5 ± 0.1

[a] F1 = 0.1: 0.02; Bud: Lec

[b] F2 = 0.1: 0.02: 0.01; Bud: CA: PL

[c] F3 = 0.2: 0.04: 0.02; Bud: CA: PL